Macromolecules

ARTICLE

pubs.acs.org/Macromolecules

Synthesis and Properties of Dendritic Emitters with a Fluorinated Starburst Oxadiazole Core and Twisted Carbazole Dendrons

Zhen-Hua Zhao, Hao Jin, Yan-Xin Zhang, Zhihao Shen,* De-Chun Zou, and Xing-He Fan*

Beijing National Laboratory for Molecular Sciences, Key Laboratory of Polymer Chemistry and Physics of Ministry of Education, College of Chemistry and Molecular Engineering, Peking University, Beijing 100871, China

Supporting Information

ABSTRACT: Three generations of novel dendrimers (G1, G2, and G3) with an electron-deficient fluorinated starburst oxadiazole core and twisted carbazoles as dendrons were synthesized via aromatic nucleophilic substitution reaction at ambient temperature by the weak base potassium fluoride with a high selectivity in a nearly quantitative yield, which was attributed to the high reactivity of the *para* fluorine atom activated by oxadiazole and multiple fluorine atoms. ^{1}H NMR, ^{19}F NMR, elemental analysis, and MALDI-TOF MS results confirmed the designed chemical structures. Varying the generation to gradually modify the dendrons could gradiently modulate the HOMO−LUMO energy band gaps of G*n*, which was verified by cyclic voltammetry results. Photoluminescent spectra showed the dual fluorescence emission of the dendrimers in solutions, which indicated that twist intramolecular charge transfer occurred between oxadiazole and carbazole separated by nonconjugated bonds. The G*n*-based devices with the configuration of ITO/PEDOT:PSS/Gn/TPBI/AlQ/LiF/Al displayed a stable green emission in their electroluminescent spectra with a gradual increase in external quantum efficiency and current efficiency for higher-generation dendrimers, owing to gradually improved charge transport. The device with G3 possessed the lowest turn-on voltage along with the highest external quantum efficiency of 1.49%, maximum current efficiency of 4.6 cd/A, and a high luminance of 4882 cd/m^2, indicating that it had the best carrier balance.

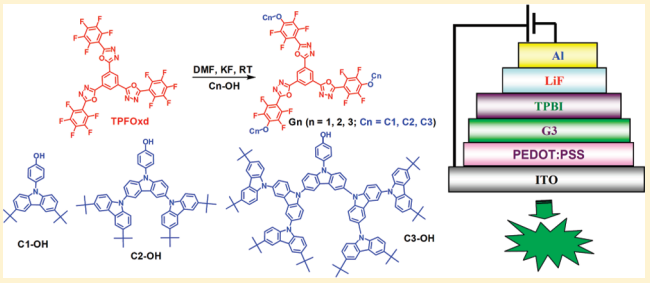

INTRODUCTION

Organic light-emitting diodes (OLEDs) have received tremendous research attention in both academic interests and potential applications for full-color flat-panel displays because of their advantages over more energy-consuming traditional displays and lighting for addressing the energy crisis.[1−3] To achieve high power efficiency of electroluminescent (EL) devices, one of the key factors is to balance charge injection from the two electrodes and efficiently transport both holes and electrons within the emitting layer.[4−6] At present, using dendrimers[7−9] in OLEDs has received tremendous research attention.[10−14] With their well-defined structures, three-dimensional spherical architectures, and site isolation effect, dendrimers possess excellent solution-processing capabilities and chemical advantages in tailoring multifunctional groups to balance charge injection and transport.

However, the use of light-emitting dendrimers containing dendrons with controllable charge transport is still in its infancy,[11] even though there have been extensive research efforts on charge-transporting dendrimers and dendrons.[15,16] Furthermore, it remains a major challenge to effectively tune the charge transport and device efficiency by simply changing the generation of dendrimers.[17−23] Moreover, the flexibility of many highly branched dendrons usually leads to poorly isolated cores susceptible to strong intermolecular interactions, and the cores are easily quenched, resulting in a low external quantum efficiency (EQE).[24−26] Consequently, using different generations of large, rigid dendrons and a nonplanar, for instance, starburst,[27] core to control charge transport and inhibit intermolecular interactions is an ideal strategy to achieve desirable emitting dendrimers with controlled charge transport. Fortunately, different generations of 3,6-cross-coupling carbazole dendrons[28,29] as hole-transporting materials have received much attention owing to their twisted configurations and gradiently tunable HOMO energy (E_{HOMO}) levels.[30] They are ideal dendrons to modulate the charge transport by varying the generation.

To address the problems mentioned above, we need to choose a highly efficient reaction route or a highly reactive functional group to synthesize novel dendritic emitters with well-defined, rigid structures and controllable charge transport. Herein, in this paper, we report the facile preparation of dendrimers by introducing starburst perfluorophenyl oxadiazole with highly reactive, thus, functional C−F bonds and additional fluorine atoms which facilitate electron transport.[31−33] Notably, the C−F bond could even react with phenols in a quantitative yield at ambient temperature in the presence of a weak base potassium fluoride as the catalyst.[34] On the basis of the above considerations, we used the

Received: November 3, 2010
Revised: January 12, 2011
Published: February 18, 2011

convergent strategy[9] to synthesize dendrimers with carbazole phenols transferring holes and starburst oxadiazole units transferring electrons. Meanwhile, the flexibility of this synthetic strategy allowed us to systematically change the generation and volume of the carbazole dendrons in the dendrimers and gradually tune the HOMO−LUMO energy band gap, leading to light-emitting dendrimers with tunable opto-electric and electrochemical properties as well as excellent thermal stability.

EXPERIMENTAL SECTION

Materials. Benzene-1,3,5-tricarboxylic acid, boron tribromide (BBr_3), and tetrabutylammonium perchlorate [$(C_4H_9)_4NClO_4$] were purchased from Acros Organics. 2,3,4,5,6-Pentafluorobenzonitrile was purchased from Zhejiang Yongtai Chemical Products Inc. and used as received. Anhydrous potassium fluoride was purchased from Beijing Chemical Reagent Co. and treated at 200 °C overnight. Anhydrous *N, N′*-dimethylformamide (DMF), toluene, and pyridine were carefully treated before use. All other chemicals and reagents were purchased from Beijing Chemical Reagent Co. and used as received.

Measurements. ^{1}H NMR and ^{13}C NMR spectra were recorded at ambient temperature on either a Bruker ARX 400 MHz spectrometer (^{1}H NMR 400 MHz and ^{13}C NMR 100 MHz) or a Varian Mercury 300 MHz spectrometer (^{1}H NMR 300 MHz and ^{13}C NMR 75 MHz) using tetramethylsilane as an internal reference. ^{19}F NMR spectra were recorded on a Varian Mercury 300 MHz (^{19}F NMR 282 MHz) using trifluoroacetic acid as an external standard. The chemical shifts were reported in the ppm scale. FTIR spectra were recorded on a Bruker Vector 22 Fourier transform infrared spectrometer. High-resolution mass spectra (HRMS) were measured on a Bruker APEX IV Fourier transform ion cyclotron resonance mass spectrometer by electrospray ionization (ESI). The MALDI-TOF MS data were obtained using on Bruker Daltonics Autoflex III MALDI-TOF spectrometer. Elemental analysis was conducted by an Elementar Vario EL instrument (Elementar Analysensysteme GmbH). UV−vis absorption spectra were measured with a Perkin-Elmer lambda 35 spectrophotometer. Photoluminescent (PL) spectra were obtained using a Hitachi F-4500 fluorescence spectrophotometer. Thermogravimetric analysis (TGA) was performed on a TA Q600 SDT instrument at a heating rate of 20 °C/min under nitrogen (100 mL/min). Differential scanning calorimetry (DSC) was recorded with a TA Q100 thermal analyzer at a heating rate of 10 °C/min under nitrogen.

Cyclic voltammetry (CV) was conducted using a CHI 630C (Shanghai Chenhua Instrument Co.) voltametric analyzer. The experiments were performed at ambient temperature in CH_2Cl_2 solutions containing 0.1 M tetrabutylammonium perchlorate as the supporting electrolyte at a scanning rate of 100 mV/s, and the detailed procedures could be found elsewhere.[35] The energy levels were calculated using the ferrocene (Fc) value of −4.8 eV with respect to the vacuum level, which was defined as zero. Two drops of Fc (1 M in CH_2Cl_2) were added, and the measured oxidation potential of Fc (vs Ag/AgCl) was 0.46 V. Therefore, the E_{HOMO} levels of the dendrimers could be calculated by the equation $E_{HOMO} = -e[U_{onset(ox)} - U_{1/2,Fc} + 4.8\ V]$ and the LUMO energy (E_{LUMO}) levels could be estimated by the equation $E_{LUMO} = -e[U_{onset(red)} - U_{1/2,Fc} + 4.8\ V]$, where $U_{1/2,Fc}$ standards for the half-wave potential of Fc/Fc^+.

Device Fabrication and Characterization. The fabrication process of the OLED devices followed a standard procedure which was described elsewhere.[35]

Synthetic Procedures. *Syntheses of the Dendrons.* The syntheses of the carbazole phenol precursors were prepared according to the literatures or modified methods which can be found in the Supporting Information, and the synthetic routes are outlined in Scheme S1 of the Supporting Information.

Synthesis of the Core TPFOxd

5-(Perfluorophenyl)-2H-tetrazole. To a stirring solution of NaN_3 (1.0 g, 15.3 mmol) in water, $ZnCl_2$ (2.1 g, 15.3 mmol) and 2 mL of acetic acid were added sequentially into a round-bottomed flask. After 10 min, 2,3,4,5,6-pentafluorobenzonitrile (3.0 g, 15.3 mmol) was added, and the mixture was refluxed for 6 h. Then it was cooled to ambient temperature and neutralized by HCl (2 mol/L) until pH = 1, followed by stirring for another 30 min. The solid was collected and further washed by water to give 2.5 g of white solid with a yield of 69%; mp =152−153 °C. ^{19}F NMR (d_6-DMSO, 282 MHz, δ): −61.7 (m, 2F), −73.9 (m, 1F), −81.0 (m, 2F). MS (EI^+): calcd $(M + H)^+/z$, 237.0; found $(M + H)^+/z$, 237.0.

1,3,5-Tris(5-(perfluorophenyl)-1,3,4-oxadiazol-2-yl)benzene (TPFOxd). To a stirring solution of 5-(perfluorophenyl)-2*H*-tetrazole (1.2 g, 5.1 mmol) in 30 mL of toluene, benzene-1,3,5-tricarbonyl trichloride (0.4 g, 1.6 mmol) and pyridine (0.37 g, 4.8 mmol) were filled into a round-bottomed flask. After being refluxed for 30 min, the mixture was cooled to ambient temperature and filtered, followed by washing with methanol and water three times to afford 0.9 g of white solid with a yield of 92%; mp = 236−237 °C. IR (KBr) ν (cm^{-1}): 3071, 2131, 1657, 1521, 1496, 1096, 994, and 836. ^{1}H NMR ($CDCl_3$, 300 MHz, δ): 9.09 (s, 3H); ^{13}C NMR ($CDCl_3$, 100 MHz, δ): 163.6, 155.7, 146.8−146.6, 145.2−145.1, 144.2−143.9, 142.6−142.3, 139.7−139.4, 137.2−136.8, 128.4, 125.8, 100.5, 100.2. ^{19}F NMR ($CDCl_3$, 282 MHz, δ): −57.0 (m, 6F), −67.7 (m, 3F), −80.9 (m, 6F). MS (EI^+): calcd M^+/z, 780; found M^+/z, 780. Anal. Calcd for $C_{30}H_3F_{15}N_6O_3$: C, 46.17; N, 10.77; H, 0.39. Found: C, 46.05; N, 10.60; H, 0.60.

Syntheses of the Dendrimers. **G1.** A mixture solution of TPFOxd (0.18 g, 0.23 mmol), 4-(3,6-di-*tert*-butyl-9*H*-carbazol-9-yl)phenol (C1-OH) (0.27 g, 0.72 mmol), and 0.10 g of anhydrous potassium fluoride in DMF was stirred under argon at ambient temperature for 8 h. The reaction solution was added dropwise into a mixture solvent of methanol and distilled water (50 mL, v/v, 1/1). The resulting precipitate was collected by filtration and thoroughly washed with methanol and distilled water twice to give 0.39 g of white solid with a yield of 90%; mp >300 °C, T_d(5 wt %) = 449 °C, T_g = 196 °C. IR (KBr) ν (cm^{-1}): 3048, 2961, 1652, 1508, 1483, 1263, 1220, 996, and 845. ^{1}H NMR ($CDCl_3$, 400 MHz, δ): 9.15 (s, 3H), 8.14 (s, 6H), 7.56 (m, 6H), 7.47 (m, 6H), 7.32−7.26 (m, 12H), 1.45 (s, 54H). ^{19}F NMR ($CDCl_3$, 282 MHz, δ): −57.6 (m, 6F), −73.5 (m, 6F). HRMS (ESI^+): calcd $(M + Na)^+/z$, 1856.6486; found $(M + Na)^+/z$, 1856.6427. Anal. Calcd for $C_{108}H_{87}F_{12}N_9O_6$: C, 70.69; H, 4.78; N, 6.87. Found: C, 70.47, H, 4.87; N, 6.85.

G2. This compound was prepared according to the procedure for the synthesis of G1 except that 4-(3′,6′-di-*tert*-butyl-6-(3,6-di-*tert*-butyl-9*H*-carbazol-9-yl)- 9*H*-3,9′-bicarbazol-9-yl) phenol (C2-OH) instead of C1-OH was added, resulting in a yellow solid with a yield of 93%; mp >300 °C, T_d(5 wt %) = 479 °C, T_g = 306 °C. IR (KBr) ν (cm^{-1}): 3047, 2960, 1652, 1507, 1489, 1220, 996, and 809. ^{1}H NMR ($CDCl_3$, 400 MHz, δ): 9.15 (s, 3H), 8.24 (s, 6H), 8.16 (s, 12H), 7.76 (d, J = 8.4 Hz, 6H), 7.61 (m, 12H), 7.45 (d, J = 8.8 Hz, 12H), 7.39 (d, J = 8.4 Hz, 6H), 7.33 (d, J = 8.8 Hz, 12H), 1.45 (s, 108H). ^{19}F NMR ($CDCl_3$, 282 MHz, δ): −57.4 (m, 6F), −73.3 (m, 6F). MALDI-TOF MS: calcd M^+/z, 3161.4; found M^+/z, 3161.8. Anal. Calcd for $C_{204}H_{177}F_{12}N_{15}O_6$: C, 77.47; H, 5.64; N, 6.64. Found: C, 77.46; H, 5.97; N: 6.44.

G3. This compound was prepared according to the procedure for the synthesis of G1 except that 4-(6-(3′,6′-di-*tert*-butyl-6-(3,6-di-*tert*-butyl-9*H*-carbazol-9-yl)-9*H*-3,9′-bicarbazol-9-yl)-3′,6′-bis(3,6-di-*tert*-butyl-9*H*-carbazol-9-yl)-9*H*-3,9′-bicarbazol-9-yl)phenol (C3-OH) instead of C1-OH was added, resulting in a yellow solid with a yield of 92%; mp >300 °C, T_d(5 wt %) = 445 °C, T_g = 367 °C. IR (KBr) ν (cm^{-1}): 3047, 2959, 1651, 1490, 1223, 996, and 809. ^{1}H NMR ($CDCl_3$, 400 MHz, δ): 9.18 (s, 3H), 8.55 (s, 6H), 8.27 (s, 12H), 8.15 (s, 24H), 7.87−7.83 (m, 12H), 7.76 (m, 6H), 7.65−7.59 (m, 24H), 7.47−7.43 (m, 30H), 7.33 (m, 24H), 1.46 (s, 216H). ^{19}F NMR ($CDCl_3$, 282 MHz, δ): −57.3 (m, 6F), −73.2 (m, 6F). MALDI-TOF MS: calcd M^+/z, 5820; found M^+/z,

5820. Anal. Calcd for $C_{396}H_{357}F_{12}N_{27}O_6$: C, 81.75; H, 6.18; N, 6.50. Found: C, 81.48; H, 6.37; N, 6.40.

RESULTS AND DISCUSSION

Syntheses of the Dendrimers. For the syntheses of the different generations of carbazole phenols as dendrons which serve as the electron donors, the intermediate compounds C1-OH, C2-OH, and C3-OH were synthesized using benzyl protection and Pd/C system rather than methyl or tosyl protecting groups by Lu et al.[29,36] The detailed synthetic procedures are depicted in Scheme S1 of the Supporting Information.

We first attempted to synthesize the core, TPFOxd, using the cyclization reaction through dehydration of bishydrazides by phosphorus oxychloride ($POCl_3$).[37−39] However, no starburst oxadiazole was formed. Then we chose an alternative, effective route to synthesize the starburst oxadiazole derivative via a tetrazole intermediate which was produced from nitrile with azide.[40−42] The detailed synthetic procedure is shown in Scheme 1. The first step involved the formation of the aromatic tetrazole, which was quantitatively generated by the corresponding 2,3,4,5,6-pentafluorobenzonitrile with sodium azide. The key step was to prepare a single pure product of the aromatic tetrazole, which was synthesized with the classical route by using zinc chloride or ammonium chloride with sodium azide. However, the *para* F of the 2,3,4,5,6-pentafluorobenzonitrile was very easily replaced by azide, and the impurities could not be easily removed by recrystallization. After adding 1−2 mL of acetic acid in the azide solution and stirring for 10 min before the nitrile was added, it could afford the pure white product by simple filtration. Then the tetrazole was treated with benzene-1,3,5-tricarbonyl trichloride, and the starburst oxadiazole derivative was obtained via Huisgen intramolecular cyclization ring transformation with a high yield and excellent purity without further purification. Although the traditional solvent was pyridine,[43] it did not work in our system even when refluxed in pyridine for a few hours. We chose anhydrous toluene as the reaction solvent and an equivalent pyridine as the base to neutralize HCl which was released by trichloride. ^{1}H NMR, ^{13}C NMR, ^{19}F NMR, MS, and elemental analysis results confirmed the designed chemical structure of the core, TPFOxd.

Subsequently, the first-, second-, and third-generation dendrimers G*n* (*n* = 1, 2, 3) were synthesized by the convergent growth method to join the presynthesized, different generations of twisted carbazole dendrons and the core TPFOxd, as also outlined in Scheme 1. Treating the TPFOxd core with phenols via the aromatic nucleophilic substitution (SN_{Ar}) reaction gave G1, G2, and G3 with an almost 100% yield. The *para* F atom with respect to oxadiazole on the pentafluorophenyl was greatly activated by the oxadiazole group and the other four fluorines, and the C−F bond could even react with phenols in a quantitative yield at ambient temperature in the presence of the weak base potassium fluoride as the catalyst. Under the weakly basic condition, phenols were converted to phenoxides, and HF was converted to potassium hydrogen difluoride with KF. The potassium hydrogen difluoride could be easily removed by washing. The efficient nature of the reaction with few byproducts allowed all G*n* dendrimers to be purified by simple precipitation. G1, G2, and G3 could be easily dissolved in common solvents, such as dichloromethane, chloroform, ethyl acetate, toluene, chlorobenzene, and so on. And the structures of G1, G2, and G3 were confirmed using ^{1}H NMR and ^{19}F NMR, elemental analysis, and HRMS or MALDI-TOF MS, etc.

Scheme 1. Synthetic Procedures for Preparation of TPFOxd and Dendrimers G1, G2, and G3

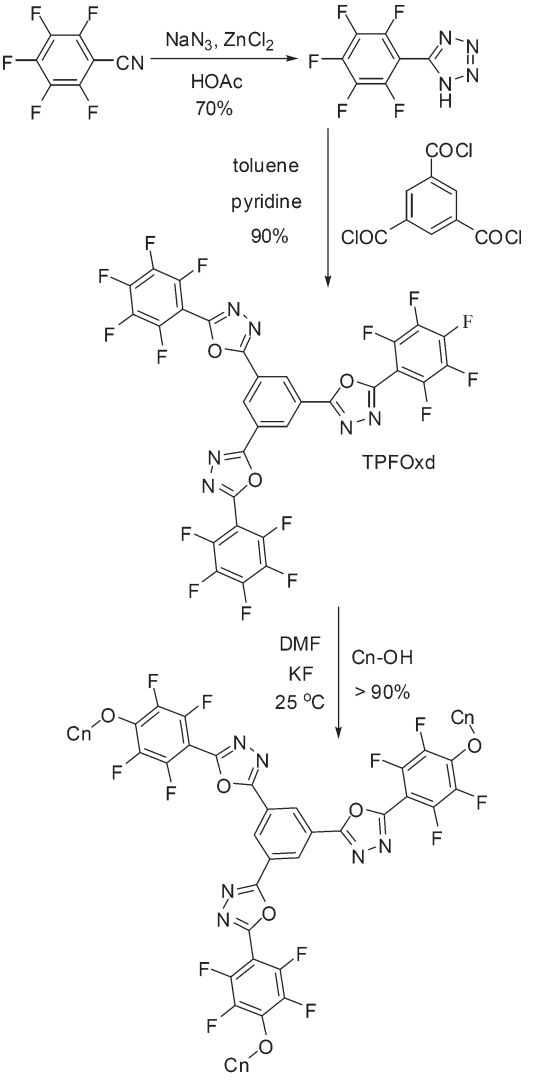

^{19}F NMR and ^{1}H NMR Results. For the ^{19}F NMR spectra in Figure 1, the resonance peak of the *para* F of TPFOxd did not appear in the spectra of G1, G2, and G3, indicating that the replacement of the *para* F atoms by phenoxides had occurred, which proceeded via the Meisenheimer complex.[44,45] The Meisenheimer complex was stabilized by the phenyl with multiple fluorines and the neighboring electron-withdrawing oxadiazole. At the same time, SN_{Ar} reaction took place at ambient temperature, attributable to the exceptional reactivity of the para F, and the low temperature prevented the *ortho* F of the oxadiazole from being substituted. Because of the large steric hindrance of the *ortho* F at ambient temperature,[45] the *para* F reacted more quickly than the *ortho* F, even though the *ortho* F was more electron-deficient. The chemical shift of *ortho* F in G1, G2, and G3 only had a negligible change; it changed from −57.6 ppm for G1 to −57.4 ppm for G2 and then to −57.3 ppm for G3, as shown in Figure 1. This trend was similar to the hydrogen shift of the phenyl group in the

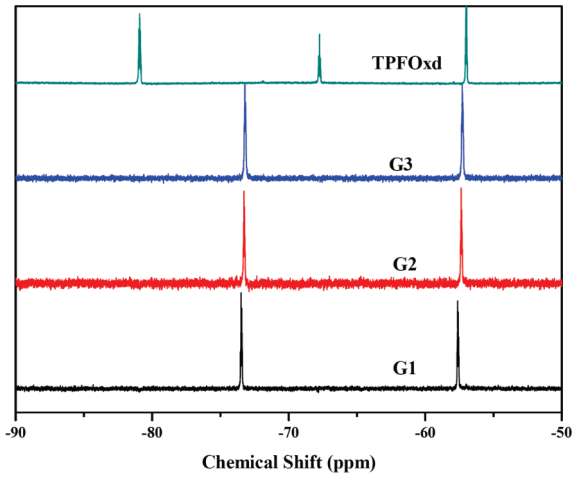

Figure 1. ^{19}F NMR spectra of G1, G2, G3, and TPFOxd.

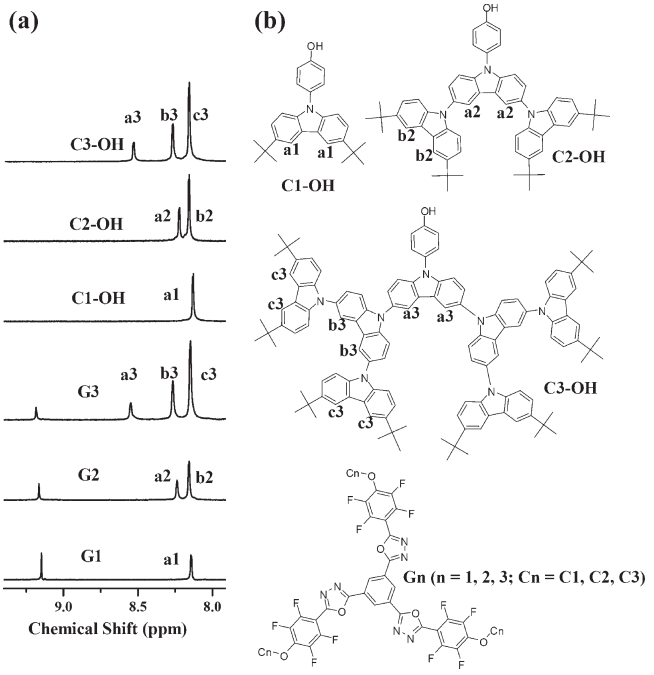

Figure 2. ^{1}H NMR spectra (a) and structures (b) of C1-OH, C2-OH, C3-OH, G1, G2, and G3.

core of G1, G2, and G3, which will be discussed in the following section.

In the ^{1}H NMR spectra, the resonance of the hydrogen at the *meta* position with respect to the N atom in the carbazole units of G3 (as shown in Figure 2) shifted from 8.15 ppm for c3 to 8.27 ppm for b3 and then to 8.55 ppm for a3, which suggested that the electron density of carbazole gradually became lower from the outermost units to the innermost one, attributable to the weak inducing effect of the outer twisted carbazoles with an antiplanar conformation.[30] The corresponding electron density of the outermost carbazole layer increased with increasing generation of the dendrimers from G1 to G3, which resulted in increasing E_{HOMO} levels for the G*n* dendrimers, in line with the CV results discussed in the next section. In the meanwhile, the shift of the hydrogens of the phenyl group in the core TPFOxd only had a slight downfield shift from 9.15 ppm for G1 and G2 to 9.18 ppm for G3, which agreed well with the negligible change of the ^{19}F NMR results, attributable to the negligible inducing effect of different carbazole dendrons on the core TPFOxd. Furthermore, these results also demonstrated that the electrons of the carbazole and oxadiazole had almost independent behaviors.

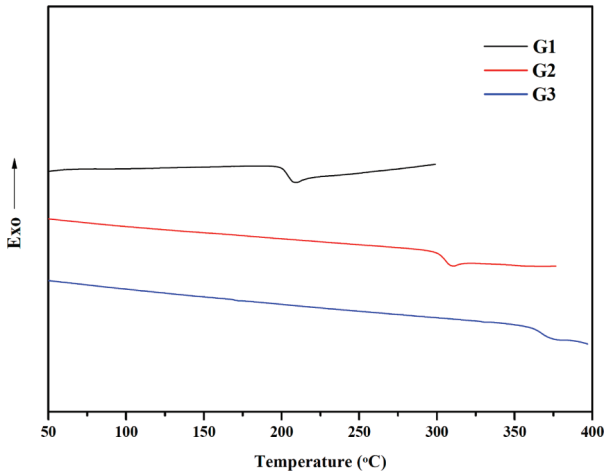

Figure 3. DSC thermograms during the second heating processes of the dendrimers.

Table 1. Electrochemical Properties of the Dendrimers Obtained from CV Measurements

sample	$U_{onset(red)}$ (V)[a]	$U_{onset(ox)}$ (V)[b]	E_g (eV)	E_{HOMO} (eV)	E_{LUMO} (eV)
G1	−1.43	1.13	2.56	−5.47	−2.91
G2	−1.45	0.97	2.42	−5.31	−2.89
G3	−1.45	0.94	2.39	−5.28	−2.89

[a] The onset voltage of the reduction process. [b] The onset voltage of the oxidation process.

Thermal Properties of Dendrimers. Thermal properties of G1, G2, and G3 were first investigated by TGA. The onset temperatures at which 5% weight loss occurred were 448, 479, and 445 °C for G1, G2, and G3, respectively. It indicated that the G*n* series had excellent thermal stability, which could be ascribed to the presence of the thermally resistant fluorine element and the oxadiazole with peripheral carbazoles. DSC results elucidated that G1, G2, and G3 had high glass transition temperatures of 204, 306, and 367 °C, respectively, as observed during the second heating process (Figure 3), which was attributed to the considerably rigid structure. The increase in T_g with increasing generation was owing to the increase in the molecular weight.[46]

Electrochemical Properties. We employed CV measurements to explore the electrochemical behavior of the dendrimers. The results are shown in Figure S1 of the Supporting Information, and the detailed data are summarized in Table 1. The oxidation peaks were originated from the peripheral carbazole units of the electron-rich dendrons. G1 only underwent a single reversible oxidation at 1.13 V, which involved a continuous one-electron oxidation process of the three outer carbazoles. G2 and G3 showed more complicated oxidation behaviors,[47] which involved two successive reversible oxidation processes. On the basis of the decreased first onset oxidation potential of G*n* (1.13, 0.97, and 0.94 V for G1, G2, and G3, respectively) with increasing generation, the E_{HOMO} levels were calculated to be −5.47, −5.31, and −5.28 eV for G1, G2, and G3, respectively. The E_{HOMO} levels of the G*n* dendrimers gradiently increased, and they were modulated by increasing the generation of the carbazole

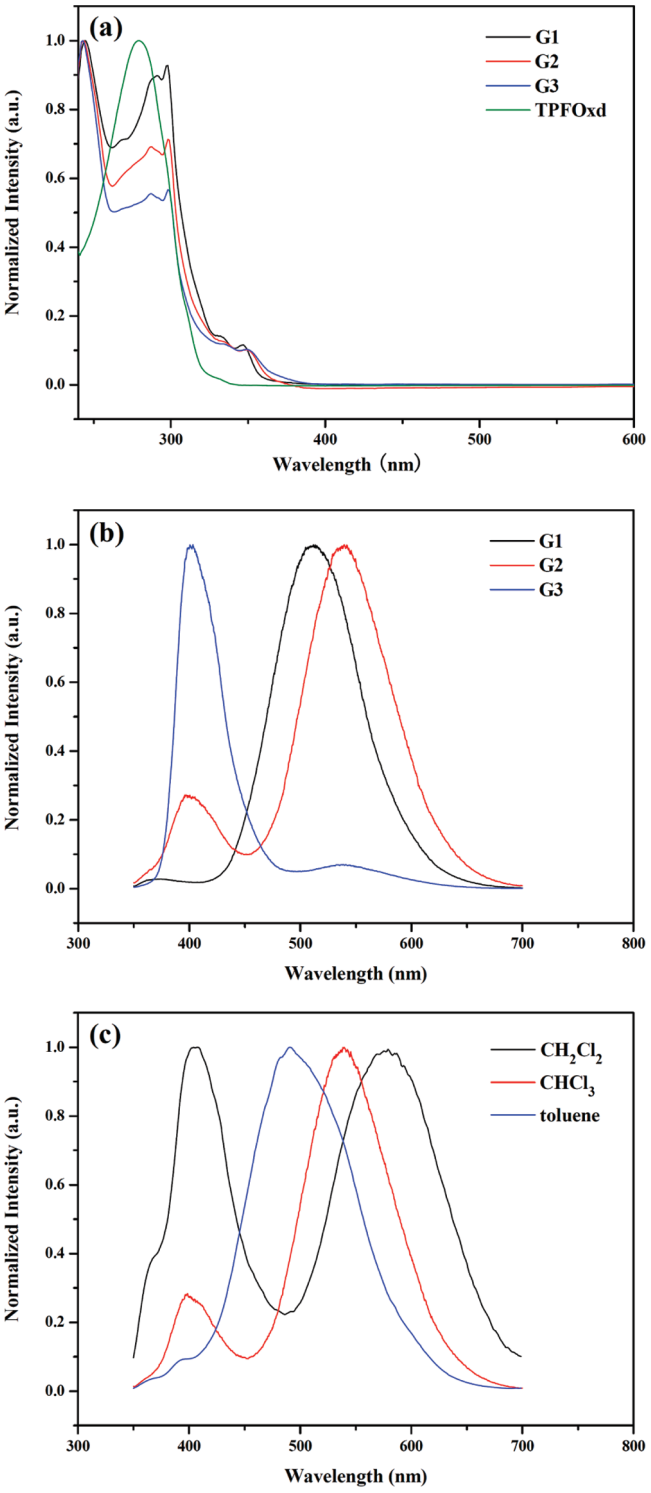

Figure 4. UV−vis absorption spectra of the G*n* dendrimers and the core (a) and photoluminescent spectra of the G*n* dendrimers (b) in $CHCl_3$ solutions (1×10^{-6} mol/L) and photoluminescent spectra of G2 in CH_2Cl_2, $CHCl_3$, and toluene (1×10^{-6} mol/L) (c).

dendrons, in line with the ^{1}H NMR results discussed in the above section.

During the negative scanning in CH_2Cl_2 solutions, an irreversible reduction process started from −1.43 to −1.45 V for G1 to G3, which corresponded to the reduction process of the electron-deficient oxadiazole units. Similarly, E_{LUMO} levels of the dendrimers

Table 2. Maximum Photoluminescent Emission Wavelength of the Dendrimers in Different Solvents and in Films

sample	CH_2Cl_2 (nm)	$CHCl_3$ (nm)	toluene (nm)	film (nm)[a]
G1	556	510	485	486
G2	578	539	490	502
G3	596	553	532	505

[a] Photoluminescent wavelength of the G*n* dendrimers in films spin-coated from toluene solutions (10 mg/mL).

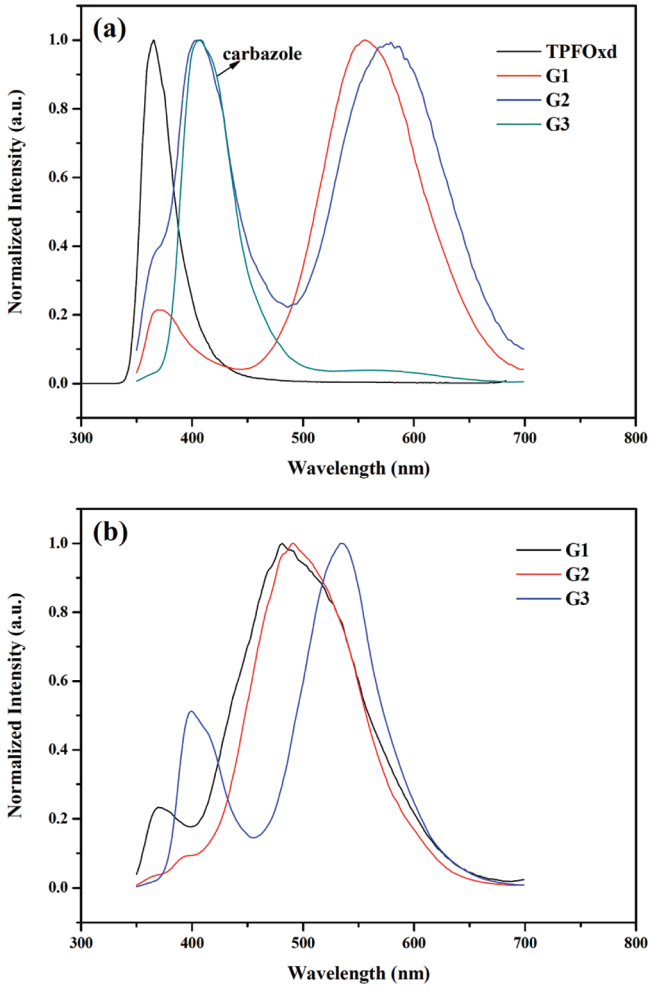

Figure 5. Photoluminescent spectra of the G*n* dendrimers and the core in CH_2Cl_2 solutions (1×10^{-6} mol/L) (a) and those of the G*n* dendrimers in toluene solutions (1×10^{-6} mol/L) (b).

were calculated to be all in the vicinity of −2.90 eV. These results indicated that the outer carbazoles had little influence on the electrochemical behavior of oxadiazole, as TPFOxd exhibited $E_{LUMO} = -(-1.42 + 4.34) = -2.92$ (eV), almost unchanged after the *para* F atoms were substituted in the G*n* dendrimers. From the HOMO and LUMO energy levels, the band gaps (E_g's) were estimated to be 2.56, 2.42, and 2.39 eV for G1, G2, and G3, respectively, which were gradually modified by varying the generation of the outer dendrons.

Photophysical Properties. The UV−vis absorption spectra of the dendrimers in $CHCl_3$ solutions were measured, as shown in Figure 4a. The spectra of G1, G2, and G3 displayed two distinct absorption bands centered at 345 and 290 nm, which

dx.doi.org/10.1021/ma1024957 |*Macromolecules* 2011, 44, 1405–1413

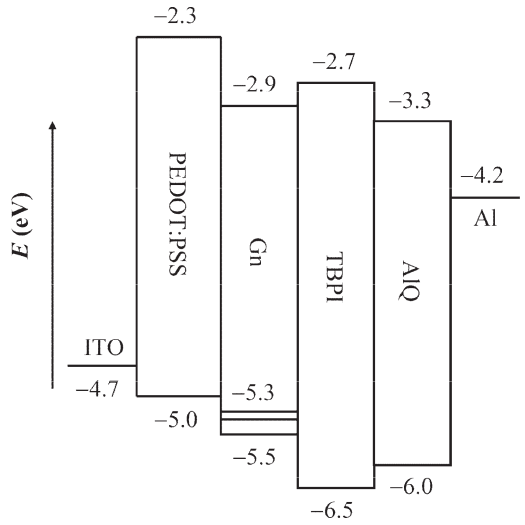

Figure 6. An estimated energy diagram.

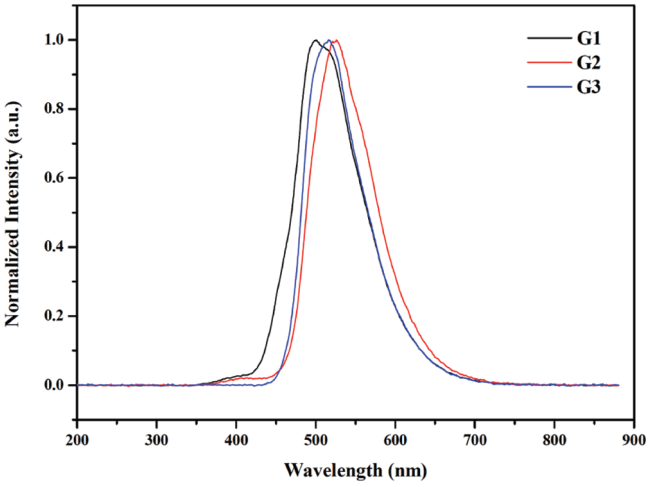

Figure 7. Electroluminescent spectra of devices **a** with the configuration of ITO/PEDOT:PSS/Gn/TPBI (15 nm)/LiF (1 nm)/Al (100 nm) at a bias voltage of 8 V.

were assigned to the carbazole moiety (345 nm) and oxadiazole (290 nm, overlapping with the carbazole absorption). In the absorption spectra of G1, G2, and G3, the cutoff absorption shifted from 445 to 448 nm. The end absorption had no significant red shift with increasing polarity of the solvent. This was attributed to the steric hindrance and the nonconjugated ether bond between carbazole and oxadiazole, and both of these factors resulted in minimized electronic coupling of the two chromophores in the ground states.

The photoluminescent spectra of the G*n* dendrimers in $CHCl_3$ solutions were measured at ambient temperature, as shown in Figure 4b. The detailed data are listed in Table 2. At a first glance, the photoluminescent spectrum of G2 in the $CHCl_3$ solution exhibited distinct dual luminescence with maxima located at 402 nm (F1 band, locally excited state) and 539 nm (F2 band). The spectra of G2 in other solvents also displayed dual luminescence, so did those of G1 and G3 in different solvents. As the concentration was increased from 1×10^{-6} to 1×10^{-4} mol/L, no aggregation bands appeared, and the emission maxima barely shifted. The F1 band, generally known as

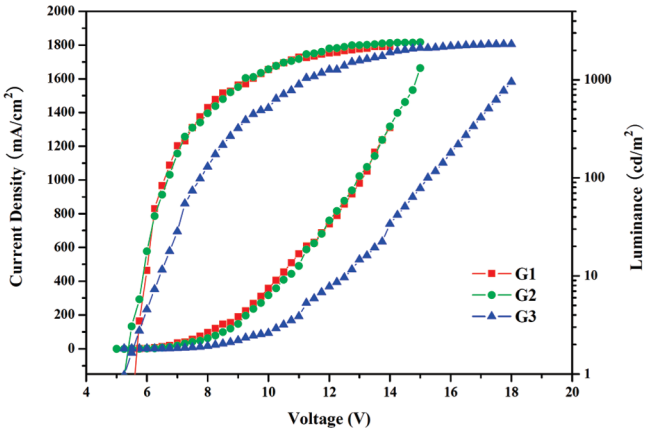

Figure 8. Luminance−current density−voltage characteristics of devices **a** with the configuration of ITO/PEDOT:PSS/Gn/TPBI (15 nm)/LiF (1 nm)/Al (100 nm).

the normal emission, could be attributed to carbazole (donor, 402 nm). Considering the rigid, bulky nature of the dendrimers, we assigned the long-wavelength emission (F2) to the intramolecular charge-transfer (ICT) emission.[48] Taking into account of the rotation of the electron-donor and electron-acceptor systems linked by C−O bonds, we reasoned that the F2 band was a twisted intramolecular charge-transfer (TICT) emission.[47,49,50] The change of the solvent polarity led to a large Stokes shift, as expected: the maximum emission wavelength of 578 nm was longer for the spectrum in CH_2Cl_2 which has a higher polarity than $CHCl_3$, while the emission blue-shifted to 490 nm in toluene with a lower polarity (Figure 4c).

Figure 5 illustrates the photoluminescent spectra of G*n* in CH_2Cl_2 and toluene solutions, and the detailed data are also summarized in Table 2. As expected with the effect of solvent polarity, the higher polarity, the longer emission wavelength. For example, the emission wavelength was 556, 578, and 596 nm in CH_2Cl_2 for G1, G2, and G3, respectively, while it blue-shifted to 480, 502, and 530 nm for G1, G2, and G3, respectively, when the solvent was changed to toluene with a lower polarity. The low intensity of the F2 band of G3 relative to those of G1 and G2 (Figures 4b and 5a) in polar solvents could be explained by the solvation effect which did not favor the twisted intermolecular charge transfer.[49,50] On the other hand, such an effect favored the F2 band (TICT) of the dendrimers in the nonpolar solvent toluene. Further, as the generation of outer dendron increased, the distance between the donor (carbazole) and acceptor (oxdiazole) was larger, resulting in the red shift of the F2 band for G3 compared with that for G1 and G2.

In addition, from photoluminescent spectra of the G*n* dendrimers in films (Figure S2 of Supporting Information) and in solutions (Figure 5b), the full widths at half-maximum (fwhm) of the spectra were narrower in the films than in corresponding toluene solutions, and no aggregation peak appeared in the spectra of films, probably ascribable to the nonplanar rigid carbazole with a 67° twist dihedral[30] as well as the difficulty in a close packing and suppressed intermolecular interactions, both of which were caused by the starburst oxadiazoles of the dendrimers.

Electroluminescent Properties of LED Devices. On the basis of their nonconjugated structures and redox behaviors, the dendrimers were expected to facilitate the transport of electrons and holes in OLED devices. We fabricated devices with appropriate configurations to match up corresponding energy

Table 3. Electroluminescent Performances of Devices a with the Configuration of ITO/PEDOT: PSS/G*n*/TPBI (15 nm)/LiF (1 nm)/Al (100 nm)

sample	U_{onset} (V)	L_{max} (cd/m^2)	η_{Imax} (cd/A)	η_{Lmax} (lm/W)	CIE coordinate	η_{extmax} (%)	λ (nm)
G1	5.6	2191	0.346	0.688	(0.23, 0.44)	0.260	501
G2	5.2	2420	0.596	1.138	(0.30, 0.56)	0.355	526
G3	5.3	2307	0.459	0.955	(0.27,0.55)	0.310	517

Table 4. Electroluminescent Performances of Devices b with the Configuration of ITO/PEDOT:PSS/G*n*/TPBI (15 nm)/AlQ (30 nm)/LiF (1 nm)/Al (100 nm)

sample	U_{onset} (V)	L_{max} (cd/m^2)	η_{Imax} (cd/A)	η_{Lmax} (lm/W)	CIE coordinate	η_{extmax} (%)	λ (nm)
G1	6.3	4758	1.018	0.532	(0.23, 0.45)	0.350	501
G2	5.6	4252	3.560	2.240	(0.30, 0.56)	0.911	522
G3	5.2	4882	4.600	2.640	(0.26, 0.57)	1.491	514

levels (Figure 6). First, devices **a** with a configuration of ITO/PEDOT:PSS/Gn/TPBI/LiF/Al were fabricated. The devices **a** with G1, G2, and G3 had low turn-on voltages (at 1 cd/m^2) of 5.6, 5.2, and 5.3 V, respectively. The electroluminescent spectra in Figure 7 showed that the major peaks fell in the green-light region. The corresponding electroluminescent spectra were similar to those of casting films (Figure S2 in Supporting Information) with much narrower emission bands, of which the main one could be attributed to the F2 band, in comparison with the photoluminescent spectra of solutions (Figure 5b), suggesting that there was no aggregation in the devices. Characteristics of current density and luminance versus bias voltage ($J-V-L$) for the devices **a** with the dendrimers are depicted in Figure 8, and the detailed data are also listed in Table 3. The device with G2 had the maximum luminance of 2420 cd/m^2, and the EQE was 0.35%. In fact, this device possessed the best performance compared with those containing G1 and G3 in both maximum luminance and efficiency, and the lower turn-on voltages could be attributed to the better carrier balance of G2.

To further demonstrate the advantages of these multifunctional dendrimers, we fabricated devices **b** containing G1, G2, and G3 with the configuration of ITO/PEDOT:PSS/Gn/TPBI/AlQ/LiF/Al. In these devices, the G*n* dendrimers functioned as both emitting materials and hole transporting materials, and the AlQ layer was introduced between the TPBI layer and the cathode to act as the electron-transporting layer because the E_{LUMO} level of AlQ was in between those of TPBI and aluminum. From the energy level diagram in Figure 6, the introduction of the AlQ layer led to a smaller energy gap between the cathode and the TPBI layer, resulting in the reduction of the electron injection barrier from the cathode to the TPBI layer. As the generation of the carbazole dendrons increased, the hole transport increased, with the turn-on voltage decreasing from 6.3 to 5.2 V, along with improved current efficiency, luminous efficiency, and EQE, as summarized in Table 4. The results in Tables 3 and 4 suggested that after the AlQ layer was introduced, there was a better carrier balance in the devices.

Furthermore, the device containing G3 had a superior performance due to the better balance of charge carriers in the device compared with those having G1 and G2. The maximum luminance was 4882 cd/m^2, luminous efficiency was 2.64 lm/W, and the EQE was 1.49%. All the devices had a green emission (Figure S3 in Supporting Information) similar to devices **a**, indicative of a stable emission region with varying generation. It is worth noting that the OLED devices remained quite stable when the bias voltage was increased from 6 to 15 V (Figure 9), ascribable to the stability of oxadiazole and carbazole as well as the high glass transition temperatures of the dendrimers.

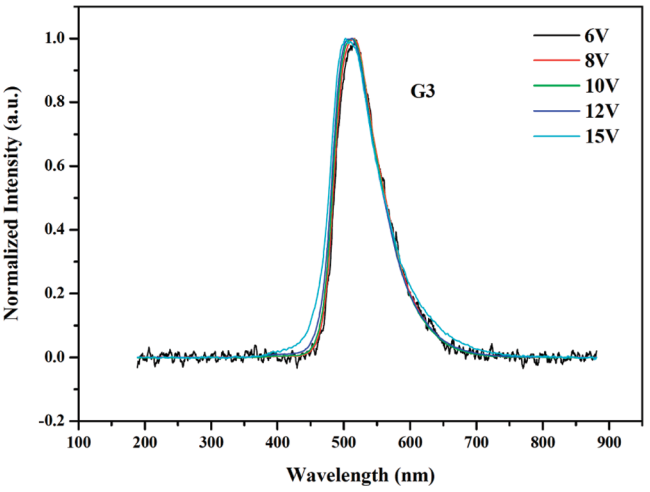

Figure 9. Electroluminescent spectra of G3 in device **b** under different voltages.

Therefore, the properties of devices **a** and **b** with the G*n* dendrimers as the emitting layer indicated that G2 itself had a better balance of charge carriers when compared with G1 and G3. On the other hand, when an electron-transporting layer AlQ was added, high-performance devices containing G1, G2, and G3 could be obtained, and the performance of the device containing G3 was superior compared with those of the devices containing the two other dendrimers G1 and G2.

Considering the moderate quantum efficiencies of the G*n* series, we could change the content of carbazole in the periphery to adjust the charge transfer. Taking advantage of the reactivity of the *ortho* fluorines with respect to oxadiazole, we could also introduce more oxadiazoles in the *ortho* positions of the starburst core. Further research on optimizing the chemical structures to adjust the balance of carriers and device architectures to improve efficiency is in progress.

CONCLUSIONS

In summary, we introduced highly active C−F bonds to synthesize a series of novel dendrimers (G1, G2, and G3) containing a starburst oxadiazole core and twisted carbazole

dendrons via SN_{Ar} reaction at ambient temperature by the weak base potassium fluoride with a high selectivity in a nearly quantitative yield. TGA results demonstrated high thermal stability owing to the presence of the rigid carbazole, multiple fluorines, and oxadiazole in the dendrimers. CV measurements along with ^{1}H NMR results indicated that the dendrimers had a gradient change of the LUMO−HOMO energy band gap due to gradual chemical modification. UV−vis absorption spectra showed that the dendrimers had almost no red shift due to the separation of the donor and the acceptor by the nonconjugated ether bonds. Photoluminescent spectra showed the dual fluorescence emission of the dendrimers in solutions, which indicated that twist intramolecular charge transfer occurred between oxadiazole and carbazole. Electroluminescent spectra showed a single-peak emission in the region of green light in the devices **a** and **b** with the configurations of ITO/PEDOT/Gn/TPBI/LiF/Al and ITO/PEDOT/Gn/TPBI/AlQ/LiF/Al, respectively. In the devices **a**, G2 had the best performance which could be attributed to a better carrier balance of the dendrimer itself. On the contrary, for devices **b** with an additional AlQ layer to transport electrons, the external quantum efficiency and maximum current efficiency gradually increased, attributable to better hole transport with increasing generation of the carbazole dendrons. The devices had low turn-on voltages. The third-generation dendrimer G3 had the highest EQE of 1.49%, maximum current efficiency of 4.6 cd/A, and power efficiency of 2.6 lm/W, accompanied by a high luminance of 4800 cd/m^2, which suggested that G3 had the best balance with AlQ in the device **b**. Because of the remarkable ability for controlling properties, we expect that the method described in this work will be of important value for preparation of high-performance OLEDs.

■ ASSOCIATED CONTENT

Supporting Information. Syntheses of intermediates **1** to **17**, cyclic voltammograms of the G*n* dendrimers, photoluminescent spectra of the G*n* dendrimers in films, and electroluminescent spectra of devices **b**. This material is available free of charge via the Internet at http://pubs.acs.org.

■ AUTHOR INFORMATION

Corresponding Author

*E-mail: fanxh@pku.edu.cn (X.-H.F.); zshen@pku.edu.cn (Z.S.).

■ ACKNOWLEDGMENT

Financial support from the National Natural Science Foundation of China (Grant 20974002) and Beijing Municipal Natural Science Foundation (Key Project from the Science and Technology Development Plans of the Beijing Municipal Commission of Education) is gratefully acknowledged.

■ REFERENCES

(1) Tang, C. W.; VanSlyke, S. A. *Appl. Phys. Lett.* **1987**, *51*, 913–915.
(2) Forrest, S. R. *Nature* **2004**, *428*, 911–918.
(3) Forrest, S. R.; Thompson, M. E. *Chem. Rev.* **2007**, *107*, 923–925.
(4) Thomas, K. R. J.; Lin, J. T.; Tao, Y.-T.; Chuen, C.-H. *Chem. Mater.* **2004**, *16*, 5437–5444.
(5) Tamoto, N.; Adachi, C.; Nagai, K. *Chem. Mater.* **1997**, *9*, 1077–1085.
(6) Kamtekar, K. T.; Wang, C.; Bettington, S.; Batsanov, A. S.; Perepichka, I. F.; Bryce, M. R.; Ahn, J. H.; Rabinal, M.; Petty, M. C. *J. Mater. Chem.* **2006**, *16*, 3823–3835.
(7) Tomalia, D. A. *Prog. Polym. Sci.* **2005**, *30*, 294–324.
(8) Vögtle, F.; Gestermann, S.; Hesse, R.; Schwierz, H.; Windisch, B. *Prog. Polym. Sci.* **2000**, *25*, 987–1041.
(9) Grayson, S. M.; Fréchet, J. M. J. *Chem. Rev.* **2001**, *101*, 3819–3868.
(10) Hwang, S.-H.; Moorefield, C. N.; Newkome, G. R. *Chem. Soc. Rev.* **2008**, *37*, 2543–2557.
(11) Burn, P. L.; Lo, S.-C.; Samuel, I. D. W. *Adv. Mater.* **2007**, *19*, 1675–1688.
(12) Li, J.; Liu, D. *J. Mater. Chem.* **2009**, *19*, 7584–7591.
(13) Lo, S.-C.; Burn, P. L. *Chem. Rev.* **2007**, *107*, 1097–1116.
(14) Qin, T.; Ding, J.; Wang, L.; Baumgarten, M.; Zhou, G.; Müllen, K. *J. Am. Chem. Soc.* **2009**, *131*, 14329–14336.
(15) Shirota, Y. *J. Mater. Chem.* **2000**, *10*, 1–25.
(16) Kulkarni, A. P.; Tonzola, C. J.; Babel, A.; Jenekhe, S. A. *Chem. Mater.* **2004**, *16*, 4556–4573.
(17) Kwok, C. C.; Wong, M. S. *Macromolecules* **2001**, *34*, 6821–6830.
(18) Chen, C.-H.; Lin, J. T.; Yeh, M.-C. P. *Org. Lett.* **2006**, *8*, 2233–2236.
(19) Lupton, J. M.; Samuel, I. D. W.; Beavington, R.; Burn, P. L.; Bässler, H. *Adv. Mater.* **2001**, *13*, 258–261.
(20) Halim, M.; Pillow, J. N. G.; Samuel, I. D. W.; Burn, P. L. *Adv. Mater.* **1999**, *11*, 371–374.
(21) Gambino, S.; Stevenson, S. G.; Knights, K. A.; Burn, P. L.; Samuel, I. D. W. *Adv. Funct. Mater.* **2009**, *19*, 317–323.
(22) Yang, Z.; Xu, B.; He, J.; Xue, L.; Guo, Q.; Xia, H.; Tian, W. *Org. Electron.* **2009**, *10*, 954–959.
(23) Devadoss, C.; Bharathi, P.; Moore, J. S. *J. Am. Chem. Soc.* **1996**, *118*, 9635–9644.
(24) Freeman, A. W.; Koene, S. C.; Malenfant, P. R. L.; Thompson, M. E.; Fréchet, J. M. J. *J. Am. Chem. Soc.* **2000**, *122*, 12385–12386.
(25) Furuta, P.; Brooks, J.; Thompson, M. E.; Fréchet, J. M. J. *J. Am. Chem. Soc.* **2003**, *125*, 13165–13172.
(26) Du, P.; Zhu, W.-H.; Xie, Y.-Q.; Zhao, F.; Ku, C.-F.; Cao, Y.; Chang, C.-P.; Tian, H. *Macromolecules* **2004**, *37*, 4387–4398.
(27) Bettenhausen, J.; Strohriegl, P. *Adv. Mater.* **1996**, *8*, 507–510.
(28) Ding, J.; Gao, J.; Cheng, Y.; Xie, Z.; Wang, L.; Ma, D.; Jing, X.; Wang, F. *Adv. Funct. Mater.* **2006**, *16*, 575–581.
(29) McClenaghan, N. D.; Passalacqua, R.; Loiseau, F.; Campagna, S.; Verheyde, B.; Hameurlaine, A.; Dehaen, W. *J. Am. Chem. Soc.* **2003**, *125*, 5356–5365.
(30) Albrecht, K.; Yamamoto, K. *J. Am. Chem. Soc.* **2009**, *131*, 2244–2251.
(31) Sakamoto, Y.; Suzuki, T.; Miura, A.; Fujikawa, H.; Tokito, S.; Taga, Y. *J. Am. Chem. Soc.* **2000**, *122*, 1832–1833.
(32) Heidenhain, S. B.; Sakamoto, Y.; Suzuki, T.; Miura, A.; Fujikawa, H.; Mori, T.; Tokito, S.; Taga, Y. *J. Am. Chem. Soc.* **2000**, *122*, 10240–10241.
(33) Facchetti, A.; Yoon, M.-H.; Stern, C. L.; Katz, H. E.; Marks, T. J. *Angew. Chem., Int. Ed.* **2003**, *42*, 3900–3903.
(34) Ding, J. F.; Day, M. *Macromolecules* **2006**, *39*, 6054–6062.
(35) Jin, H.; Xu, Y.; Shen, Z.; Zou, D.; Wang, D.; Zhang, W.; Fan, X.; Zhou, Q. *Macromolecules* **2010**, *43*, 8468–8478.
(36) Xu, T.; Lu, R.; Liu, X.; Zheng, X.; Qiu, X.; Zhao, Y. *Org. Lett.* **2007**, *9*, 797–800.
(37) Kraft, A. *Chem. Commun.* **1996**, 77–79.
(38) Wang, C.; Jung, G.-Y.; Hua, Y.; Pearson, C.; Bryce, M. R.; Petty, M. C.; Batsanov, A. S.; Goeta, A. E.; Howard, J. A. K. *Chem. Mater.* **2001**, *13*, 1167–1173.
(39) Shi, W.; Qian, X.; Song, G.; Zhang, R.; Li, R. *J. Fluorine Chem.* **2000**, *106*, 173–179.
(40) Verheyde, B.; Dehaen, W. *J. Org. Chem.* **2001**, *66*, 4062–4064.
(41) Demko, Z. P.; Sharpless, K. B. *J. Org. Chem.* **2001**, *66*, 7945–7950.

(42) Bettenhausen, J.; Strohriegl, P. *Macromol. Rapid Commun.* **1996**, *17*, 623–631.
(43) Wong, K.-T.; Ku, S.-Y.; Cheng, Y.-M.; Lin, X.-Y.; Hung, Y.-Y.; Pu, S.-C.; Chou, P.-T.; Lee, G.-H.; Peng, S.-M. *J. Org. Chem.* **2005**, *71*, 456–465.
(44) Sun, Y.-M.; Wang, C.-S. *Polymer* **2001**, *42*, 1035–1045.
(45) Sato, N.; Tanaka, K.; Masaki, S.; Yamazaki, S.; Kimura, K.; Nishichi, A. *J. Polym. Sci., Part A: Polym. Chem.* **2007**, *45*, 2855–2866.
(46) Wong, K. T.; Lin, Y. H.; Wu, H. H.; Fungo, F. *Org. Lett.* **2007**, *9*, 4531–4534.
(47) Loiseau, F.; Campagna, S.; Hameurlaine, A.; Dehaen, W. *J. Am. Chem. Soc.* **2005**, *127*, 11352–11363.
(48) Curutchet, C.; Mennucci, B. *J. Am. Chem. Soc.* **2005**, *127*, 16733–16744.
(49) Rettig, W. *Angew. Chem., Int. Ed. Engl.* **1986**, *25*, 971–988.
(50) Grabowski, Z. R.; Rotkiewicz, K.; Rettig, W. *Chem. Rev.* **2003**, *103*, 3899–4032.